DESIGN AND RF MEASUREMENTS OF AN X-BAND ACCELERATING STRUCTURE FOR LINEARIZING THE LONGITUDINAL EMITTANCE AT SPARC

D. Alesini[1], A. Bacci[3], P. Chimenti[1], V. Chimenti[1], A. Clozza[1], A. Falone[2], V. Lollo[1], M. Migliorati[2], A. Mostacci[2], F. Palpini[2], L. Palumbo[2], B. Spataro[1]

[1])INFN-LNF Via E. Fermi 40, I-00044 Frascati, Italy

[2])INFN-LNF and Università degli Studi di Roma "La Sapienza", Dip. Energetica, Via A. Scarpa 14, 00161, Roma, Italy

[3])INFN-LASA di Milano Via Fratelli Cervi 201, 20090 Segrate (MI), Italy

Abstract

The paper presents the design of an X-band accelerating section for linearizing the longitudinal phase space in the Fractal Linac Coherent Light Source (SPARC). The nine cells structure, operating on the π standing wave mode, is fed by a central coupler and has been designed to obtain a 42 MV/m accelerating gradient. The 2D profile has been determined using the electromagnetic codes Super fish and Oscar-2D while the coupler has been designed using HFSS. Bead-pull measurements made on a copper prototype have been done and the results are illustrated and compared with the numerical ones. Mechanical details of the realized prototype and RF properties of the structure as a function of the assembly characteristics are also discussed.

1   INTRODUCTION

The main goals of the SPARC[1] injector project are:

1)   the generation of a high brightness electron beam able to drive a self-amplified spontaneous free-electron laser (SASE-FEL) experiment in the green visible light;

2)   the development of an ultra-brillant beam photo-injector needed for the future SASE-FEL based X-ray sources.

The SPARC photo-injector layout, reported in Fig. 1, consists of:

a)   1.6 cell RF gun of the BNL/UCLA/SLAC type[2] operating at S-band with incorporated metallic photo-cathode (Cu or Mg) and generating a 6 MeV beam;

b)   two accelerating sections of the SLAC type (S-band, travelling wave).

The beam parameter list at the end of the injector is reported in Table 1.

In the SPARC phase II the first LINAC section, downstream the RF gun, will be used to study RF compression[3]. These tests of RF compression assume great relevance in the SPARC R&D program[4] since the general layout for SPARX[5] foresees the use of a mixed compression scheme: RF compression in the photo-injector up to 500 A and one single stage of magnetic compression at 1 GeV up to the final peak current of 1 kA. In this case the use of the X-Band structure operating at 11.424 GHz is required to compensate the non-linearity distortions due to the RF curvature during acceleration and compression[6]. The schematic layout is reported in Fig 2. The X-Band structure, designed[7] to obtain 42 MV/m accelerating gradient, is a nine cells π-mode structure fed by a central coupler. The fourth harmonic of 2.856 GHz (instead of the third harmonic) has been chosen for space availability reasons and also because the technologies in the X-Band power sources and modulators have been already developed at KEK, SLAC and Varian[8-15] for future linear collider projects. The design of the accelerating section is described in par. 2. In the third paragraph of this paper we describe the copper prototype and the measurement setup while in the last paragraph we discuss the RF measurement results.
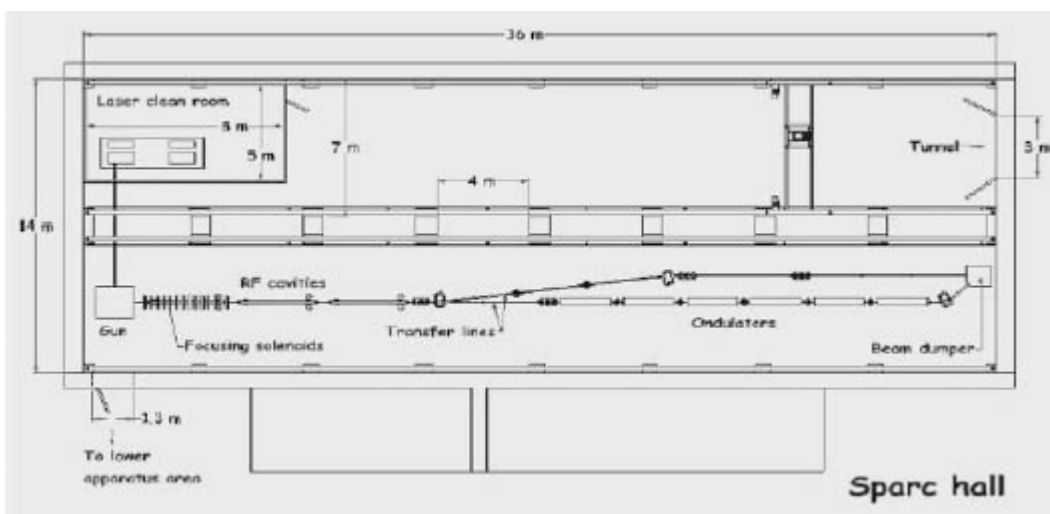

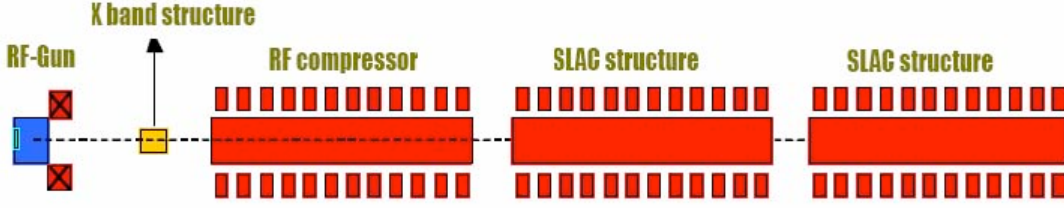**FIG. 1:** SPARC photo-injector layout.

FIG. 2: schematic layout of the photo-injector of SPARC phase II.

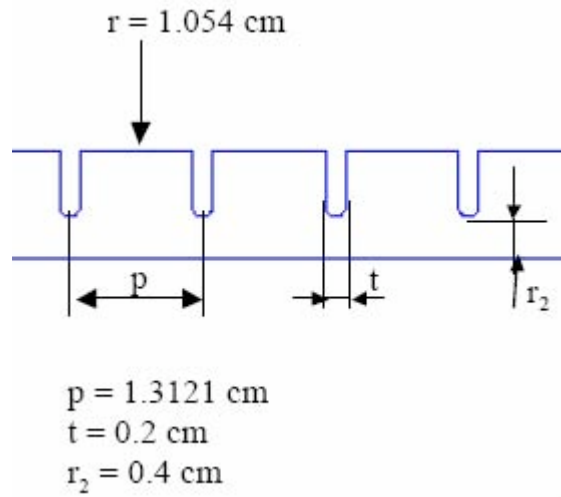**TAB.1**: beam parameter list at the end of the SPARC injector.

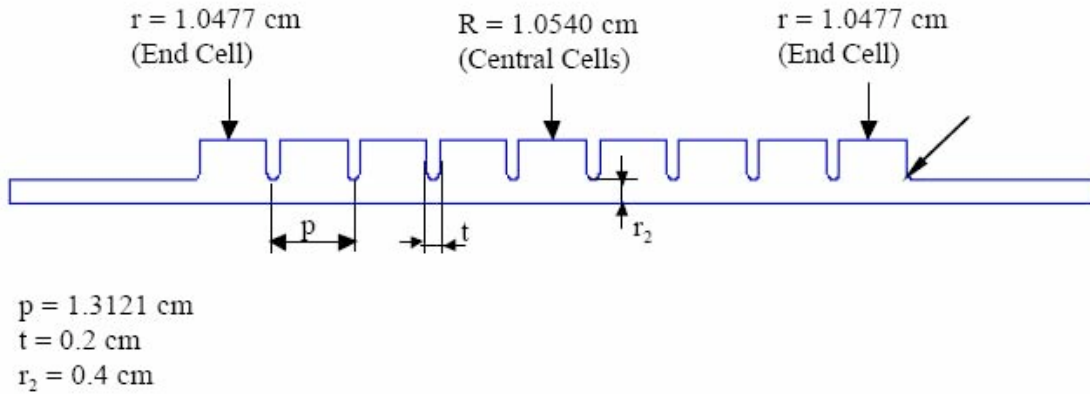|	
Electron Beam energy [MeV]	155
Bunch charge [nC]	1.1
Repetition rate [Hz]	10
Cathode peak field [MV/m]	120
Peak solenoid field [T]	0.273
Photocathode spot size [mm]	1.13
Laser pulse duration [ps]	10
Bunch energy @ gun exit [MeV]	5.6
Bunch peak current @ linac exit [A]	100
RMS normalized transverse emittance @ linac exit [mm mrad]	<2
RMS slice normalized transv. emit. @ linac exit (300 μm) [mm mrad]	<1
RMS longitudinal emittance @ linac exit [deg keV]	1000
RMS energy spread [%]	0.2
RMS bunch length @ LINAC exit [mm]	1

2 THE X BAND STRUCTURE DESIGN

2.1 2D Profile

The detailed analysis of the structure design without coupler is reported elewhere[7]. The single cell dimensions are reported in Fig. 3 and have been determined with the 2D electromagnetic (e.m.) codes Superfish[16] and Oscar-2D[17]. In particular the beam aperture diameter (r_2) has been fixed by beam dynamics requirements and the outer diameter (r) has been chosen to tune the resonance of the π-mode at 11.424 GHz.
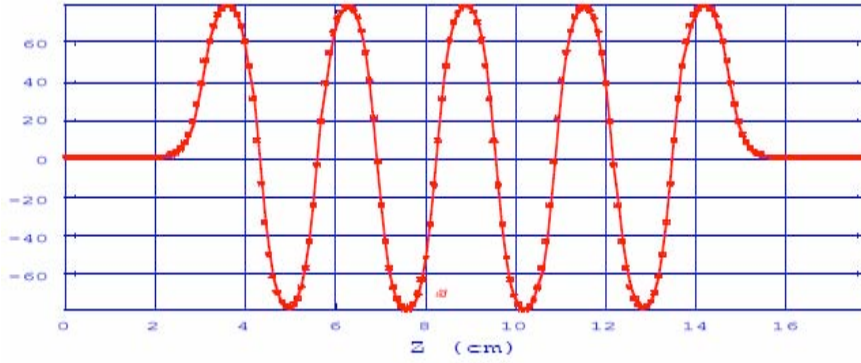
The complete structure (without coupler) is reported in Fig. 4. The choice of 9 cells has been done to achieve a total accelerating voltage V=5 MV with 3 MW of peak input power. The two cells connected to the beam pipe tube have different outer dimensions in order to compensate the detuning of the resonant frequency due to the presence of the beam pipe itself. No dedicated dampers of the parasitic higher order modes have been adopted since the X-Band structure operates on single bunch. The longitudinal electric filed on axis is reported in Fig. 5 while the cavity parameters are reported in Table 2.

r = 1.054 cm

p = 1.3121 cm
t = 0.2 cm
r_2 = 0.4 cm

FIG. 3: single cell dimensions of the π-mode X-band structure.

r = 1.0477 cm
(End Cell)

R = 1.0540 cm
(Central Cells)

r = 1.0477 cm
(End Cell)

p = 1.3121 cm
t = 0.2 cm
r_2 = 0.4 cm

FIG. 4: complete π-mode X-band structure without coupler.

**FIG. 5:** longitudinal electric filed on axis (Superfish and Oscar 2D calculations).

TAB. 2: X-band cavity parameters (Superfish and Oscar 2D calculations)

|	
Frequency [GHz]	11.424
Cells length [mm]	13.12
Number of cells	9
Beam holes radius r [mm]	4
Iris Thickness t [mm]	2
Transit time factor T	0.731
Quality factor Q	8400
R/Q [Ω/m]	9165
Coupling coefficient K [%]	2.42
Peak input power P [MW]	2.7
Duty cycle	10^{-4}
Repetition frequency [Hz]	50
Average power dissipation P_d [W]	270
Peak axial electric field [MV/m]	57.5
Kilpatrick factor	1.197
Peak surface electric field [MV/m]	105

2.2   COUPLER DESIGN

Concerning the coupler design, it has been decided to feed the cavity in the central cell in order to not excite the mode $8/9\pi$ that has the frequency nearest to the π mode and zero field in the central cell. Therefore with a central coupler we have a much greater separation of the modes and, consequently, the working mode is less perturbed by the closest one. To reduce the coupler window dimensions we have decided to taper the smaller dimension

($10.16\,mm$) of the standard X-band waveguide ($10.16\,mm \times 22.86\,mm$) to the dimension of 4 mm (Fig. 6). The coupling cell is sketched in Fig. 7.
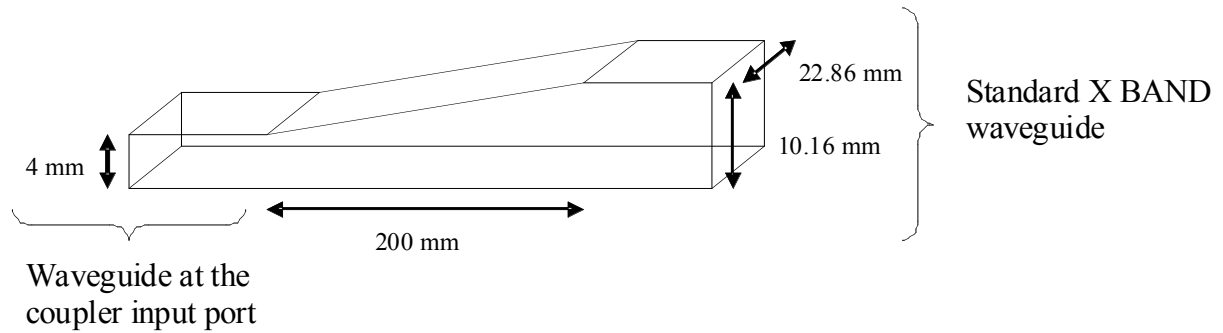
FIG. 6: tapering between the standard X-Band waveguide and the coupler input port.
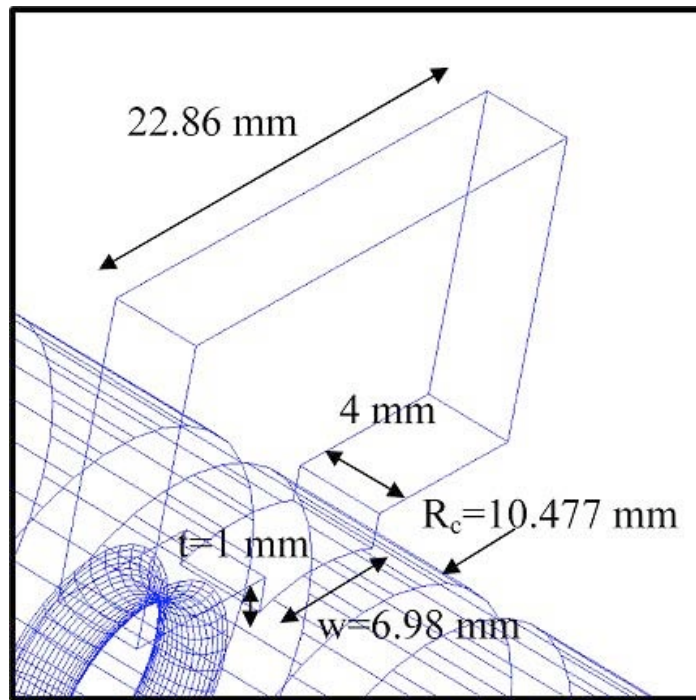

FIG. 7: sketch of the coupling cell.

The dimension of the coupler window (w) and of the central cell radius (R_c) have been tuned in order to obtain simultaneously a coupling coefficient $\beta = 1$, a resonant frequency of the whole system (cells+coupler) equal to 11.424 GHz and to preserve a good field flatness. This has been done using the e.m. code HFSS[18] by following two steps:

1)   we have simulated a single cell with coupler as shown in Fig. 8. To get a better accuracy results we have simulated only one quarter of the structure with the proper boundary conditions. The dimensions of the coupler window and cell radius have been tuned in order to obtain a coupling coefficient $\beta = 9$ (exactly 9 times the coupling coefficient that we would reach with the complete structure) and a cell resonant frequency equal to 11.424 GHz;

2)   we have simulated the complete structure (one quarter of the structure as shown in Fig 9) with the dimensions found in the previous case and we have slightly adjusted the dimensions of the coupler cell and window to obtain a good field flatness at the resonant frequency of 11.424 with $\beta = 1$.
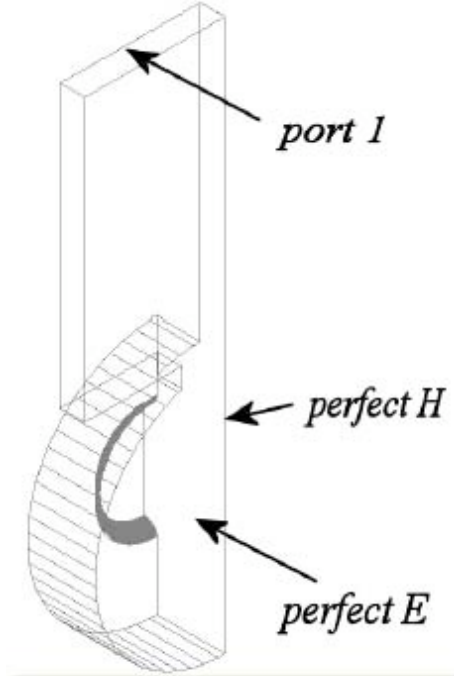
**FIG. 8:** single cell with coupler simulated by HFSS.
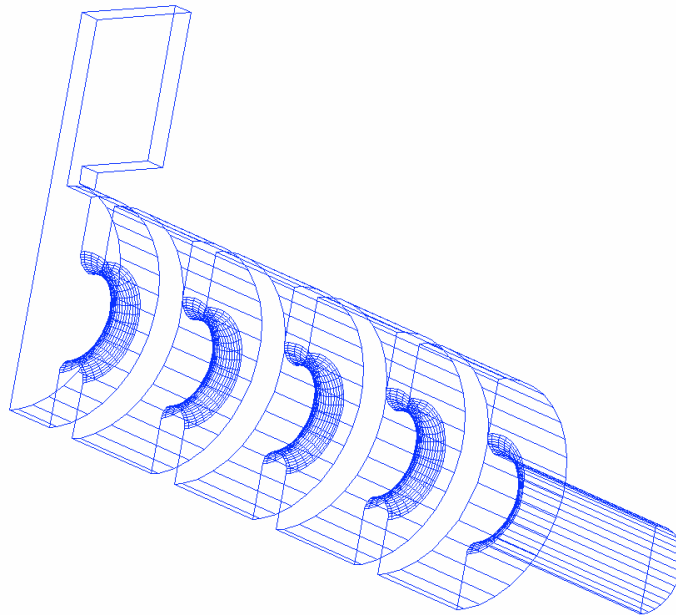
FIG. 9: complete structure with coupler simulated by HFSS.

The final cell coupler dimensions are reported in Fig. 7 and the obtained reflection coefficient at the coupler port and the electric field on axis are reported in Fig. 10. By fitting the reflection coefficient at the input coupler port with the formula:

$$|S_{11}| = \sqrt{\frac{\left(\frac{1-\beta}{1+\beta}\right)^2 + (Q_L \delta)^2}{1 + (Q_L \delta)^2}} \quad \text{with} \quad \delta = \frac{\omega}{\omega_{res}} - \frac{\omega_{res}}{\omega} \quad Q_L = Q_{EXT} \frac{\beta}{1+\beta}$$

we have obtained the external quality factor Q_{EXT}=7900 and the coupling coefficient $\beta = 1.09$. The values of the simulated Q_{EXT} and field flatness have been considered a good point to be eventually optimized after experimental measurements results.
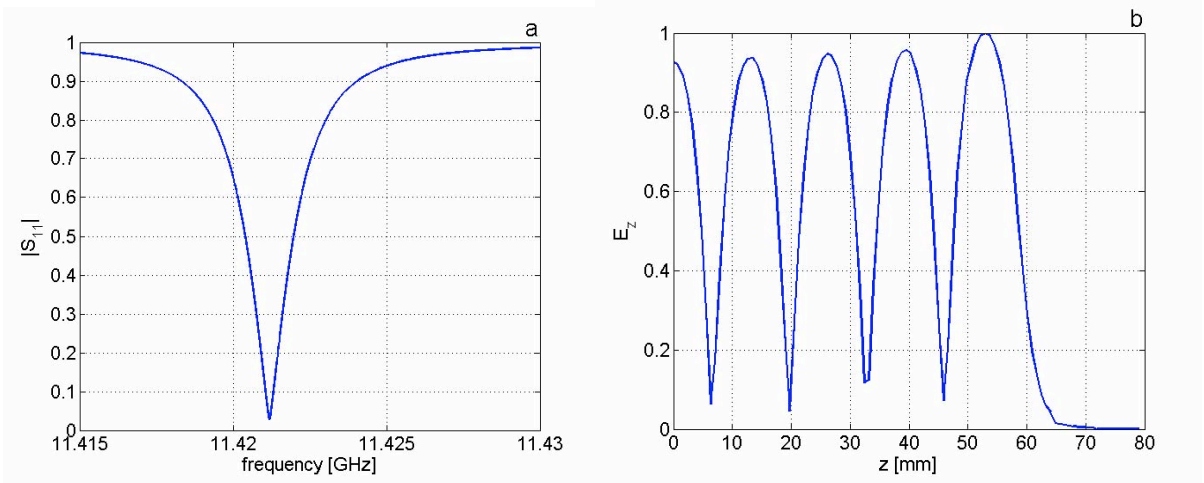
FIG. 10: simulated reflection coefficient at the coupler port and Electric field on axis at the π -mode resonant frequency (HFSS simulations).

## 3   COPPER PROTOTYPE AND MEASUREMENT SETUP

A full scale copper prototype has been constructed and is shown in Fig 11. The detail of the mechanical drawing is reported in Fig. 12. The nine cells structure has been designed for brazing, but the RF tests refer to a mechanically joined structure. The material used to build this prototype is oxygen free copper. The structure has been realised by mechanical machining with a numerically controlled lathe and the obtained precision is below ±0.01 mm, while the surface roughness is not worst than $0.4\,\mu R_a$. The surface finishing was obtained directly by mechanical machining with custom cutting tools, avoiding any polishing technique and only silicon and sulphur free cutting fluid was used. The final machining was done at constant temperature in order to guarantee as much as possible the uniformity of the mechanical dimension of the cells. After machining, a standard cleaning procedure was

performed using an alkaline solution at 3% at 50 °C followed by a rinse in tap water and a final rinse in distilled water followed by a chemical cleaning with citric acid solution and a rinse in tap water and finally a rinse in distilled water. Then the pieces were dried in a dust free oven.

FIG. 11: copper prototype of the X band structure.
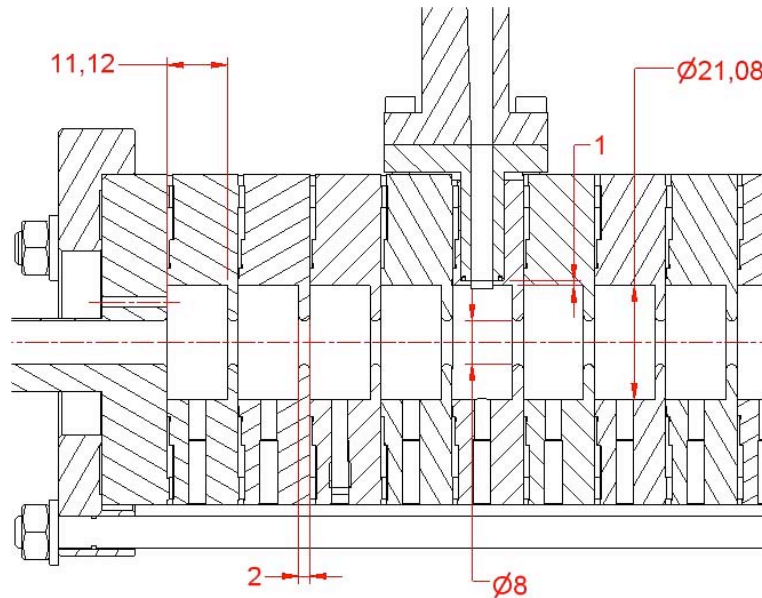
FIG. 12: detail of the mechanical drawing.

Each cell dimension has been checked with a quality control test.

The assembling procedure foresees the joining of the nine cells using two stainless steel disks used to press the structure by means of three 8 mm diameter copper rods. A torque of 5 Nm corresponds to a pressure of roughly 80 N/mm^2. To feed the structure there are also two lateral small antennas.

Two types of different measurements have been done:

1) transmission (or reflection) scattering coefficient measurement between the two antennas or between the antennas and the central coupler;

2) bead pull measurements.

With the first type of measurements we have found the resonant frequency, the β coefficient at the input ports and the unloaded or external quality factors of π (or other) mode(s). With the second type of measurements we have found the longitudinal electric field on axis and we have calculated the shunt impedance of the structure.

The complete measurement setup is shown in Fig. 13. The PC controls both the network analyzer Agilent N5230A (interfaced by a GPIB Ethernet device) and the control circuit of the steeping motor through Labview[19]. The nylon wire is kept straight by a 75 g weight.
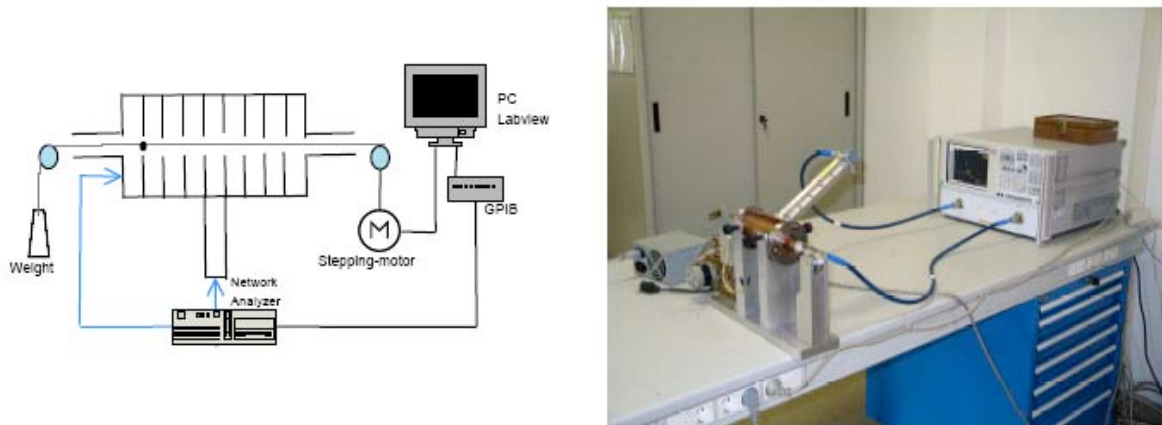
FIG. 13: picture of the measurement setup (b) and conceptual scheme (a).
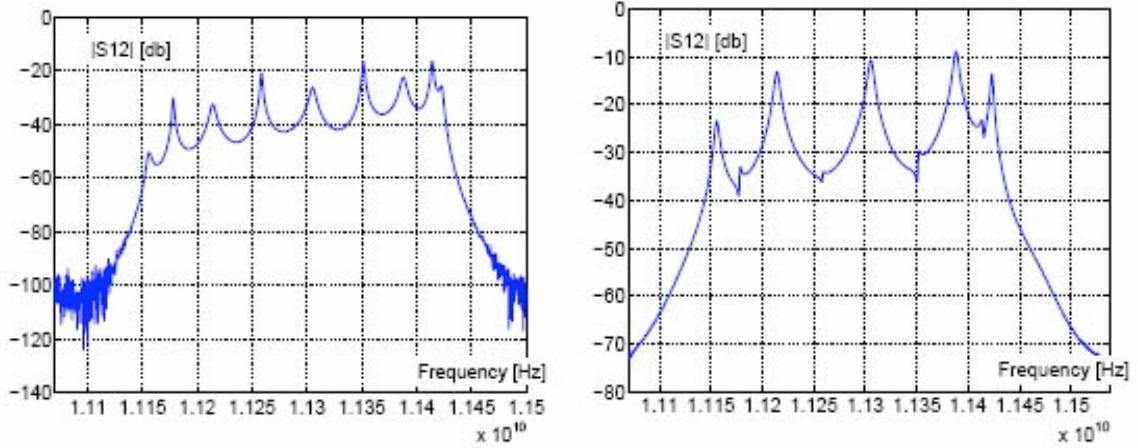
4   MEASUREMENTS RESULTS

4.1   Resonant frequency and quality factors measurements results

The transmission coefficient between the two small antennas and between the antenna and the central coupler are reported in Figs 14a and b. As previously observed, we can excite only five over nine possible modes by the central coupler because we impose a non-zero field in the central cell. On the contrary with the two antennas we can excite all the possible modes. The measured dispersion curve, compared with the one obtained from HFSS and SUPERFISH, is reported in Fig 15.

The quality factor of the resonance has been measured as a function of pressure realized by the rods. The results are reported in Fig 16. As expected the Q factor increases with the increasing pressure and, with the maximum pressure, we have obtained the result reported in
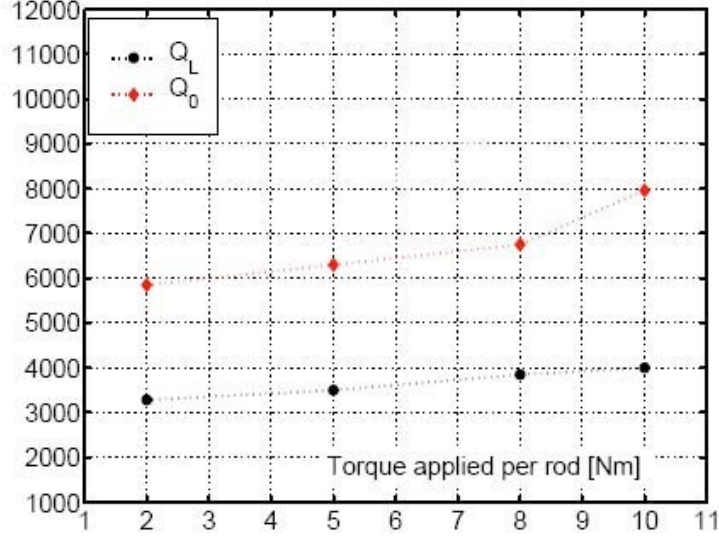
Table 3 and compared with the numerical one. These results prove that even if the structure is not brazed the electric contact is good enough to have a Q-factor of the resonance comparable with the numerical one. Concerning the external quality factor it has been found the value Q_{EXT}=8000 in agreement with the simulation results.

FIG. 14: transmission coefficients between the two small antennas (a) and between the antenna and the central coupler (b).
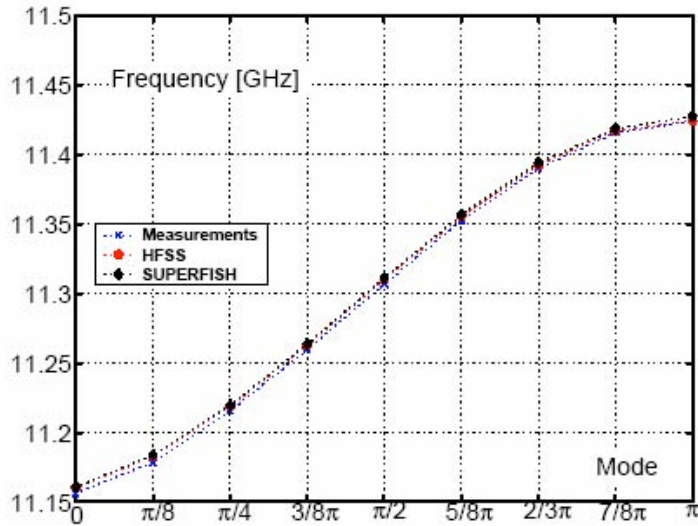
FIG. 15:: measured dispersion curve, compared with the one obtained from HFSS and SUPERFISH.

FIG. 16: measured quality factor of the π mode resonance as a function of pressure realized by the rods.

TAB. 3: unloaded quality factor measured with the maximum pressure and compared with the numerical results.

	HFSS	SUPERFISH	OSCAR 2D	Measurements
Q_0	8500	8070	8413	7960

4.2   ELECTRIC FIELD MEASUREMENT RESULTS

The bead-pull technique that we have used is based on the Slater theorem and is widely discussed elsewhere[20]. The small perturbing object inside the cavity induces a frequency shift that is related to the variation of the electric and magnetic energy stored in the cavity in the point where the object is located according to the formula:

$$\frac{\omega_p - \omega_0}{\omega_0} = \frac{1}{4U} \int_{\Delta V} \left(\mu_0 |\vec{H}|^2 - \varepsilon_0 |\vec{E}|^2 \right) dV$$

Considering the accelerating mode and the small transverse dimensions of the perturbing object (of the order of 0.1 mm) it is possible to find the longitudinal electric field on axis by the formula:

$$\frac{\omega_p - \omega_0}{\omega_0} = -\varepsilon_0 k_e \Delta V \frac{E_z^2}{4U}$$

where k_e is the form factor of the object, ΔV is the perturbing object volume, U the total energy stored in the cavity, Q_L is the loaded quality factor of the resonance and $\phi(f_0)$ is the phase of the transmission coefficient between two ports coupled with the field in the cavity. The latest expression have been written because it is more convenient to measure the phase shift of the resonant frequency instead of $\Delta\omega$ [21]. The perturbing objects are cylinders made of copper with a radius of 0.09 mm and length of 0.7 mm and 0.9 mm (measured with a digital callipers with an uncertainty of $10\,\mu m$).

A careful optimization of the measurement setup has been done in order to minimize the systematic errors and to better understand the uncertainty of the measurements. The most important reasons of induced errors in the measurements were:

1) the effect of wire nylon that induced an unwanted perturbation in the frequency measurement. To cancel this systematic error different measurements have been done with different nylon wire diameters. A typical phase resonance measurement with different wire diameters is reported in Fig. 17. The best results have been obtained with the smallest wire and the final small systematic error has been completely cancelled considering the frequency shift with and without the perturbing object. As example in Fig. 18 it is reported the results of phase shift considering different pieces of nylon wire with the smallest diameter of 0.083 mm without perturbing object;

2) the effect of the drops of glue used to fix the perturbing object. It gave a perturbation in the frequency measurement of the order of 10% of the total frequency variation. In particular the frequency variation at the center of the irises didn't go to zero. To take into account this effect different measurements have been done in order to subtract the systematic perturbation to the measure as shown in Fig. 19;

3) the effect of jitter in the longitudinal coordinate between different measurements and within a single measure. This problem, given by the stepping motor, has been reduced using a weight no more than 75 g, and correcting off-line the measurement results. As example in Fig. 20 it is reported the result of two different measurement.
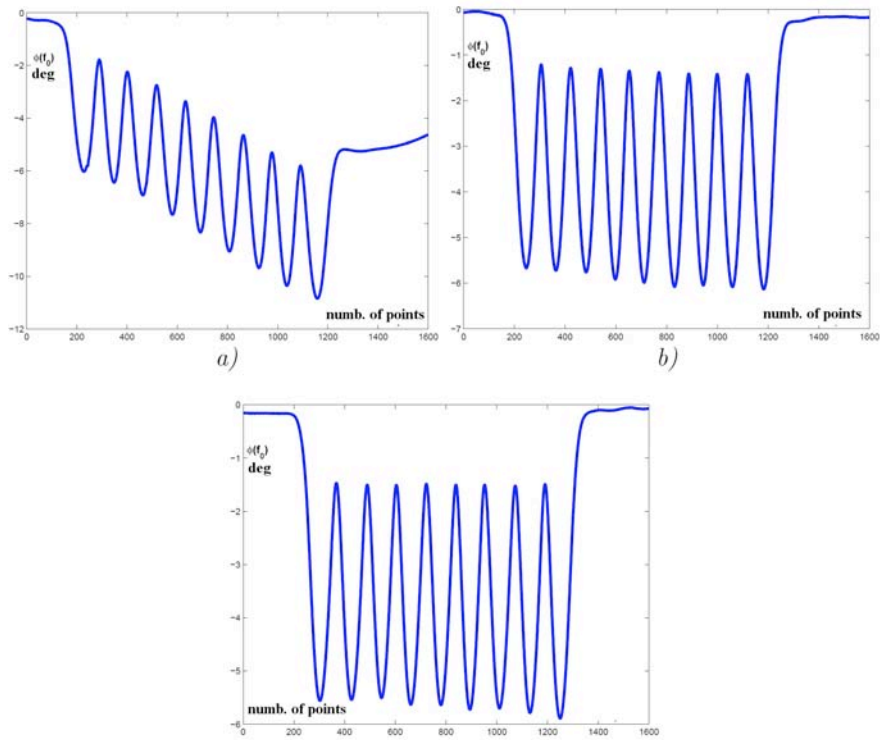
FIG. 17: phase of resonance measurement with different wire diameters: a) 0.18 mm; b) 0.148 mm; c) 0.083 mm;
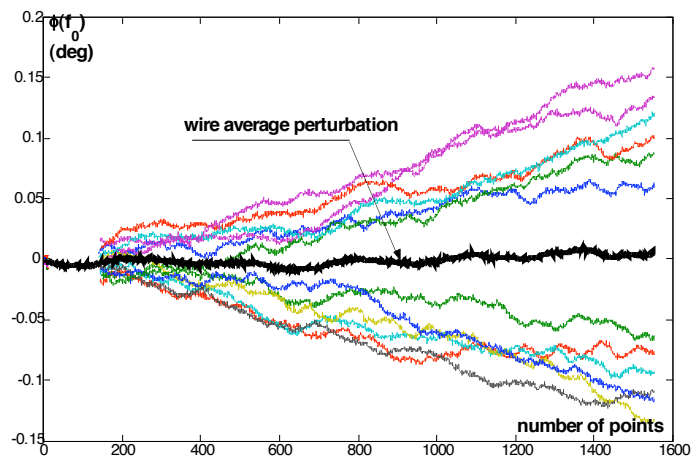
FIG. 18: resonance phase shift considering different pieces of nylon wire with the smallest diameter of 0.083 mm.
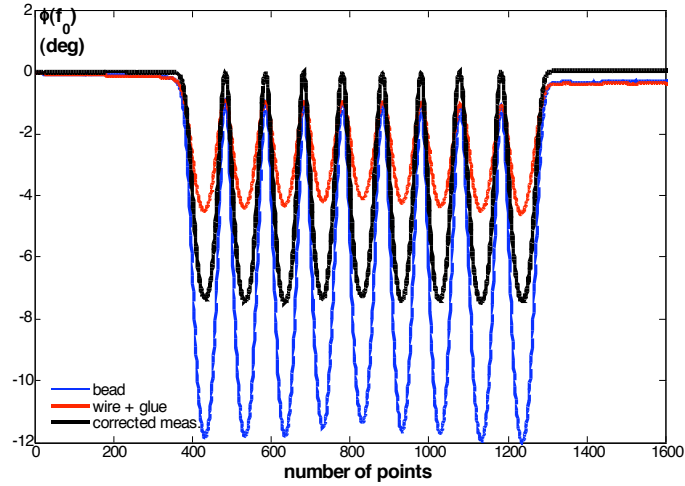
FIG. 19: phase measurement taking into account the effect of the wire and of the glue.
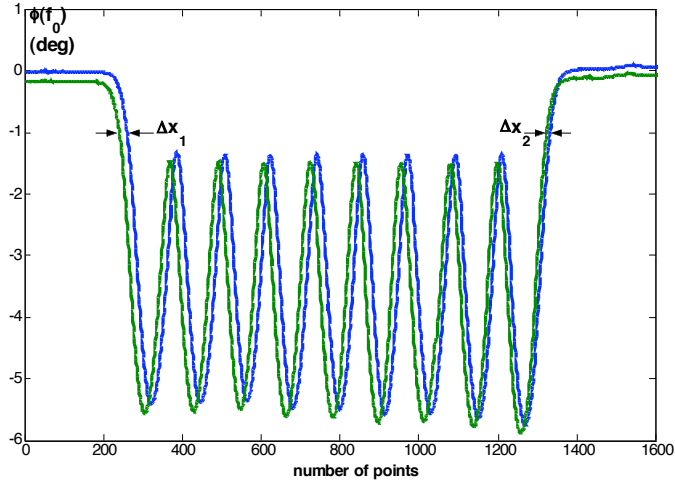

FIG. 20: jitter between two different measurements

To calculate the R/Q of the structure it has been necessary to determine the form-factor of the different perturbing objects. In literature there are many analytical formulas for the determination of the form-factor for ellipsoid geometries[22]. The used perturbed objects are far to be perfect ellipsoid and we have preferred to determine the form factor through experimental calibration[23]. Using Slater's theorem we can calibrate the form factor comparing the perturbation induced by the perturbing object in a cavity with known field with the analytical result. For this purpose, it has been used a pill-box cavity working at 1.91 GHz on the TM $_{010}$ mode. Using different resonant mode of the pillbox cavity we have also checked that the form-factor does not depend on the frequency. The results of this calibration are reported in Table 4 where the obtained form factors of two objects with different length are reported[23].

The measured longitudinal electric filed on axis, after the tuning procedure, is plotted in Fig. 21. The reached field-flatness is of the order of 1% at the nominal resonant frequency of 11.424GHz.

The calculated R_{sh}/Qs normalized to the cavity length are reported in Table 4 and is in very good agreement with the simulation results.
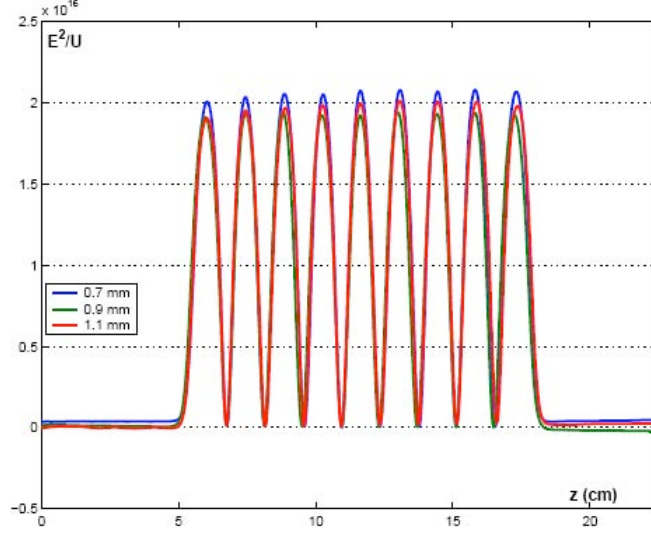
FIG. 21: measured longitudinal electric field on axis.

TAB. 4: form factors obtained by calibration of two objects with different length.

Object length [mm]	Form factor k_e	R/Q [Ω / m]
0.7	25.860 ± 0.031	9480 ± 96
0.9	28.400 ± 0.027	9367 ± 211

6   CONCLUSIONS

In the paper we have presented the design of the X-band accelerating section for linearizing the longitudinal phase space in the Frascati Linac Coherent Light Source (SPARC). The structure, operating on the π standing wave mode, is a 9 cells structure feed by a central coupler and has been designed to obtain a 5 MV accelerating voltage. Quality factors, resonant frequency and electric field measurements have been done on a copper prototype. Even if the prototype is not brazed the reached quality factors are very close to the theoretical ones. Concerning the electric field measurement with the bead pull technique we have discussed the most important reasons of induced errors and how to cancel these effects. In particular the effect of wire nylon, drops of glue used to fix the perturbing object and the effect of jitter in the longitudinal coordinate have been discussed. To calculate the R/Q factors

the perturbing objects have been calibrated with a simple pill-box and the final results are in very good agreement with the numerical ones.

Brazing tests are now in progress in the LNF for the construction of the final device.

7   REFERENCES

(1)   Technical Design Report for the SPARC Advanced Photo-Injector. Technical report, LNF-INFN, ROMA, (2003).

(2)   D.T. Palmer, The next generation photoinjector, PhD.Thesis, Stanford University.

(3)   M. Ferrario et al., Homdyn Study for the LCLS RF Photoinjector , SLAC-PUB 8400.

(4)   D. Alesini et al., Conceptual Design of a High-Brightness Linac for Soft X-ray SASE-FEL Source, these proceedings.

(5)   D.Alesini et al. (The SPARX study group), Conceptual design of a high brightness linac for soft X-ray SASE-FEL source, NIM-A, 507 (2003), pp. 502-506.

(6)   P.Emma X-band RF harmonic compensation for the linear bunch compression in the LCLS. SLAC, LCLS-TN-01-1 2001

(7)   A. Bacci et al., An X-band structure for a longitudinal emittance correction at SPARC. SIS-Pubblicazioni, LNF-INFN, LNF 03/008(R), (2003).

(8)   K. Takata, Proc. First Workshop on Japan Linear Collider (JLC),KEK, Oct. 24-25, 1989.

(9)   J.W. Wang and G.A. Loew,"Measurements of ultimate Accelerating Gradients in the SLAC

(10)   Disk-loaded Structure," 1985 PAC, Vancouver, B.C., May 1985, SLAC-PUB-3597, March 1985.

(11)   J. W.Wang, V. Nguyen-Tuong and G.A. Loew, " RF Breakdown Studies in a SLAC Diskloaded Structure," Proceedings of the 1986 Linear Accelerator Conference, Stanford, Ca, June 1986, SLAC-PUB-3940, April 1986.

(12)   J. W. Wang and G.A. Loew,"Progress Report on New RF Breakdown Studies in an S-band Structure at SLAC,"presented at the 1987 PAC,Washington,D.C.,March 1987, SLAC-PUB- 4247,February 1987.

(13)   E. Tanabe,J. W. Wang and G.A. Loew, "Voltage Breakdown at X-band and C-band Frequencies, "Proceedings of the 1986 Linear Accelerator Conference, Stanford, Ca, June 1986.

(14)   J. W. Wang,"RF Properties of Periodic Accelerating structures for Linear Colliders", SLACReport-339, July 1989.

(15)   J. R. Rees, "A Perturbation Approach to Calculating the behavior of Multi-cell Radiofrequency Accelerating Structures" PEP-255, Stanford Linear Accelerator Centre (1976).

(16)   Poisson Superfish, James H. Billen and Lloyd M. Young, software produced under U.S. Government by Los Alamos National Laboratory, Particle Accelerators 7 (4), 213-222 (1976).

(17)   P. Fernandes and R. Parodi," LALAGE – A Computer Program to Calculate the TM Modes of Cylindrically Symmetrical Multicell Resonant Structures",PAC 1982,Vol. 12, pp. 131- 137.

(18)   www.ansoft.com

(19)   LABVIEW

(20) J.C.Slater L.C.Maier Field Strenght Measurements in Resonant Cavities Journal of Applied Physics, 23 No.1, 1952.

(21) Measurement of resonant frequency and quality factor of microwave resonators Journal of Applied Physics,84 No.6,1998.

(22) G.Dome F.Caspers Precise Perturbation measurement of Resonant Cavities and Higher Mode Identi¯cation, Cern SPS/85-46,(1984).

(23) J.C.Slater Microwave Electronics, Dover Publication (1969).

(23) Guide to the expression of uncertainty in measurement. (1993).